The promoting effect of Ce on Ag/ZrO2 catalyst for the total oxidation of toluene into CO2 in the presence of water vapor

Rimeh Ismail, Jihène Arfaoui, Zouhaier Ksibi, Abdelhamid Ghorbel, Gérard Delahay

The promoting effect of Ce on Ag/ZrO_2 catalyst for the total oxidation of toluene into CO_2 in the presence of water vapor

Rimeh Ismail [1]*, Jihène Arfaoui [1], Zouhaier Ksibi [1], Abdelhamid Ghorbel[1], Gérard Delahay [2]

[1] Laboratory of Materials Chemistry and Catalysis LR01ES08, University of Tunis El manar, Campus Universitaire Farhat Hached d'El Manar, 2092, Tunis, Tunisia,

[2] ICGM, University of Montpellier, ENSCM (MACS), CNRS, Montpellier, France

*** Corresponding author: Rimeh Ismail**

ORCID: 0000-0001-5608-4715

rimeh.ismail@fst.utm.tn

Abstract

The development of advanced catalysts to reduce volatile organic compounds (VOCs) is of significant environmental and economic importance. In this work, toluene was chosen as a representative of VOCs because of its high toxicity to human health. Silver-based catalysts Ag/ZrO_2 and Ag/Ce-ZrO_2 with 2 wt.% Ag and 10 wt. % Ce were prepared for the low temperature total oxidation of toluene (C_7H_8) in the presence of water vapor. The effect of cerium species on physicochemical properties and catalytic activity in the toluene oxidation of mesoporous catalysts were investigated. The new Ag/Ce-ZrO_2 material possesses the highest catalytic activity in the total oxidation of toluene at low temperature in comparison to Ag/ZrO_2. 100% C_7H_8 conversion to CO_2 is achieved between 300 and 550 °C. It reveals that the oxygen species presented in Ag/Ce-ZrO_2 are the key factor in toluene oxidation. Silver species increases the amount of surface lattice oxygen species and leads to the migration of lattice oxygen, which effectively facilitates the low-temperature conversion of toluene oxidation.

Keywords: mesoporous catalyst, Ag/Ce-ZrO_2, total oxidation of toluene, water vapor

Graphical abstract:

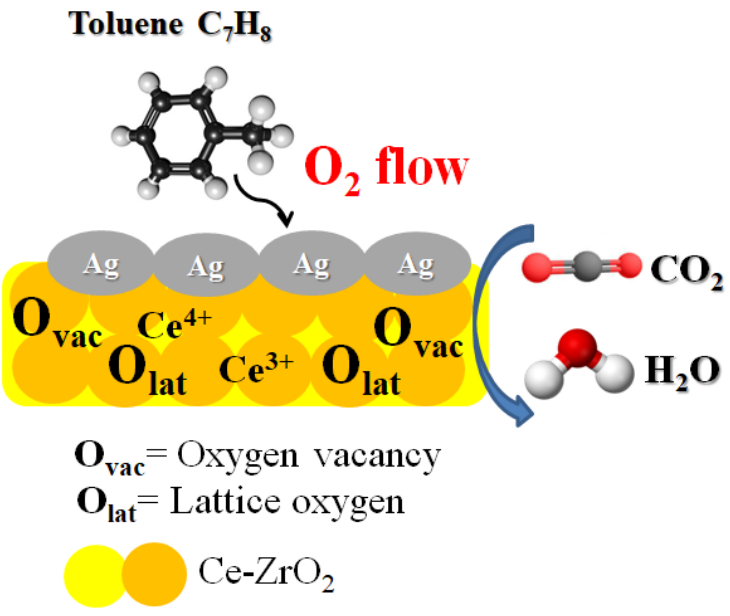

1. Introduction

Toluene, which is a cancerogenic volatile organic compound (VOC) and a typical tail gas pollutant, could pose a variety of environmental and human health effects [1]. It is considered as the precursors of complex air pollution and harmful to ecological circumstances by accelerating ozone depletion and photochemical smog [2-4]. As a result, effective elimination of toluene is required. Several technologies, such as adsorption, plasma, photocatalysis and catalytic oxidation, have been used for removing VOCs [5-11]. Among them, catalytic oxidation has been recognized as an attractive process due to its higher efficiency, selectivity and less energy consumption, the desired reaction products are carbon dioxide (CO_2) and water (H_2O) since they are not harmful for the environment [12-15]. Hence, the efforts for catalytic degradation of VOCs have been pursued by many researchers. Catalysts based on transition metal oxide [16-18] and noble metals (Pd, Pt and Au) [19-22] have been extensively studied. Nevertheless, the high cost and easy aggregation of noble metal catalysts limits their application. Thus, a small amount of noble metal supported on the transition metal oxide could be a good choice, which can not only reduce the price of the catalyst but also improve the performance of the catalyst. In this context, Ag@Pd core-shell structure supported on layered MnO_2 was studied by Li et al. [23]. The results demonstrated that the catalyst exhibited great toluene oxidation performance. Previous studies [24-25] indicated that Fe-based MOFs and ln2S3/UiO-66 exhibiting good photocatalytic activity for the degradation of tetracycline. Our previous work [26-27] revealed that Ag/ZrO_2 $Ag/Fe\text{-}ZrO_2$ and $Fe\text{-}ZrO_2$ exhibited a good catalytic activity and selectivity for the oxidation of toluene in the presence of water vapor. Additionally, Ag/MnO_2 is prepared by liquid phase reduction method for efficient toluene degradation [28].

Among the diverse transition metal oxide, cerium oxide (CeOy) is a rare earth element with good redox behavior and excellent oxygen storage capacity. These properties make CeOy have great application potential. A great number of researches have paid attention to mixed metal oxides based on Cerium for toluene oxidation [29-32]. Mn-Ce binary metal oxides were used for catalytic oxidation of toluene [29,30]. The results proved that Mn-Ce showed excellent performance than MnOx and CeOy in oxidation of toluene. $3MnOx\text{-}1CeO_y$ catalysts were performed by Chen et al. [29] by using hydrolysis driving redox. The results showed that (3Mn1Ce) demonstrated good activity for blended aromatic VOCs (chlorobenzene, benzene, toluene and xylene). Especially, 3Mn1Ce catalyst exhibited great water resistance for toluene oxidation at 280 °C. Zhang et al. [31] synthesized Ce-Mn-Ox catalysts by different methods. The authors reported that the CM-HT prepared by the hydrothermal method exhibited the best catalytic performance (T90 = 246 °C) and water resistance for toluene oxidation. Luo et al. [32] proved that Ce1Mn2 exhibited better catalytic performance (T90= 245 °C) for toluene oxidation than MnO_2 and CeO_2.

Herein, we have developed new $Ag/Ce\text{-}ZrO_2$ catalysts, containing 2 wt.% Ag and 10 wt.% Ce, for the total oxidation of toluene in a wide temperature range (200-550 °C). This work focuses on studying the effect of cerium species on the surface, structure, acidic and redox properties and performing $Ag/Ce\text{-}ZrO_2$ catalyst in the total oxidation of toluene in the presence of water vapor. ZrO_2 and Ag/ZrO_2 systems previously reported [26] were shown in this paper only to be considered as reference materials.

2. *Experimental*

2.1. Chemicals and materials

Zirconium (IV) butoxide ($Zr(OC_4H_9)_4$, Sigma-Aldrich, 80 %), anhydrous ethanol (C_2H_6O, Aldrich, 99.8 %), ethyl acetoacetate ($C_6H_{10}O_3$, Fluka, > 99.5%), $Ce(NO_3)_3$,6 H_2O (Sigma-Aldrich, ≥ 98.5 %), HNO_3 and $AgNO_3$ aqueous solutions were used in the experiment for the preparation of materials.

2.2. Preparation of materials

Sol- gel and impregnation methods are used to prepare the materials, using similar procedure to that reported in our previous work [26]. A brief description of the preparation proceeds: ZrO_2 and Ce-ZrO_2 supports were synthesized by the sol-gel route. $Zr(OC_4H_9)_4$ was dissolved in ethanol (C_2H_6O), then, ethyl acetoacetate ($C_6H_{10}O_3$) was added to the mixture. After continuous stirring at room temperature, until reagents were completely dissolved, a dilute solution of HNO_3 (0.1 M) was added drop-wise, according to the molar ratio H_2O/Zr =10, followed by stirring until the gel was formed. After that, the formed gel was dried in the autoclave, using the supercritical drying process of ethanol (T = 243 °C and P = 63 bar). The same methodology was used to obtain Ce-ZrO_2. Theoretical loading of cerium (10 wt.%) was added to the mixture before hydrolysis. Finally, the obtained materials (ZrO_2 and Ce-ZrO_2) were calcined for 3 h at 550 °C.

ZrO_2 or Ce-ZrO_2 materials were mixed with a certain amount of $AgNO_3$ aqueous solution at room temperature to obtain Ag/ZrO_2 and Ag/Ce-ZrO_2 (silver loading was fixed in a value of 2 wt.%). The samples were dried overnight at 100 °C and finally calcined at 550 °C for 3 h.

2.3. Catalyst Characterization

We used the following techniques to characterize the samples. N_2 adsorption-desorption at 77 K, X-ray diffraction (XRD), X-ray photoelectron spectroscopy (XPS), Temperature-programmed reduction (H_2-TPR), Temperature-programmed desorption (NH_3-TPD), Temperature programmed desorption of O_2 (O_2-TPD) and UV-vis spectroscopy (UV-Vis).

N_2 adsorption-desorption isotherms were collected at 77 K, using a Micromeritics Asap 2000 Analyser. The specific surface area was calculated using the Brunauer-Emmett-Teller (BET) method and the pore size distribution curves were determined by the Barrett-Joyner-Halenda (BJH) method. Each sample was degassed at 250 °C until a static vacuum of 3 $\times 10^{-5}$ bar was reached. X-ray diffraction (XRD) patterns were determined by Brüker AXS D8 diffractometer with CuKα radiation (λ = 1.5406 Å) in the 2θ range between 15° and 70° (the step size of 0.02°). The X-ray photoelectron spectroscopy (XPS) data was recorded by ESCALAB 250 of thermo electron to determine the chemical state and component of the samples. The binding energies were calibrated internally by the carbon deposit C1s binding energy (BE) at 284.6 eV. The curves were resolved using a Gaussian function. Diffuse reflectance UV-Vis spectra in 200-800 nm were studied with a spectrometer Lambda 40, Perkin Elmer, operating at room temperature. Temperature-programmed reduction (H_2-TPR) analysis was performed using an AUTOCHEM 2920 (Micromeritics) equipped with a TCD detector. The samples (80 mg) were reduced in a flow of 5 vol.% H_2 in Ar (30 cm^3/min). The temperature was increased from 50 to 800 °C at a heating rate of of 10 °C/min. The temperature programmed desorption (TPD) was used to study the acidic properties of the samples by utilizing a Micromeritics AUTOCHEM 2910. Before TPD measurements, all the prepared samples (80 mg) were pre-treated at 550 °C (ramp 10 °C/min) for 2 h under air flow (30 cm^3/min). Then, NH_3 adsorption was done at 100 °C using 5 vol.% NH_3 in He (flow rate = 30 cm^3/min) for 30 min and then flushed with He (30 cm^3/min) during 30 min to remove the physiosorbed ammonia. The temperature was ramped from 100 to 550 °C at 10 °C/min. Temperature programmed desorption of O_2 was also investigated on

the same instrument (a Micromeritics AUTOCHEM 2910). Before O_2 adsorption, the sample (80 mg) was previously activated using the same procedure for NH_3-TPD. After being cooled down to 50 °C by exposition to 5 vol% O_2 in He (flow rate = 15 cm^3/min), the sample was flushed with He (15 cm^3/min) during 17 min and finally heated between 50 and 550 °C with a heating rate of 10 °C/min.

2.4. Catalytic activity studies

Toluene oxidation measurement was done, using similar experimental conditions to that reported in ref [26, 27].

3. Results and discussion

3.1. N_2 Adsorption-desorption at 77 K

N_2 adsorption-desorption isotherms and the pore size distribution of catalysts are shown in Fig. 1 (A) and Fig. 1 (B), respectively. The textural properties of the catalysts are summarized in Table 1. As it can be seen (table 1), all the solids, calcined at 550 °C, possess high specific area (>100 m^2/g) and larger porosity (0, 28 cm^3/g) showing a good thermal stability of materials. The slight decrease of the S_{BET} and V_{PT} of ZrO_2 and Ce-ZrO_2 supports after the addition of silver is connected with the blockage of some pores of catalytic supports by silver particles, as reported in our previous work [26].

Table 1. Textural properties of the studied samples.

Sample	BET surface area (m^2/g)	Total pore Volume (cm^3/g)	Average Pore diameter (Φpore , Å)
ZrO_2	107	0,33	88
Ce-ZrO_2	119	0,35	87
Ag/ZrO_2	76	0.24	97
Ag/Ce-ZrO_2	73	0,31	127

Fig. 1A shows the N_2 adsorption-desorption isotherms and BJH pore size distribution curves of samples. All the solids exhibit type IV isotherm, indicating the presence of mesopores, with hysteresis loops type H1 or H2 (According to the IUPAC classification) [33]. H2 type, obtained for ZrO_2 and Ce-ZrO_2, is related to ink-bottle pores [34] but, H1 type, observed for Ag/ZrO_2 and Ag/Ce-ZrO_2, is characteristic of materials consisted of agglomerates (assemblages of rigidly joint particles) or compacts of approximately spherical particles arranged in a fairly uniform way [35]. The change in the pores size of ZrO_2 (Fig. 1B) proves the existence of strong interactions between the support and the supported active species.

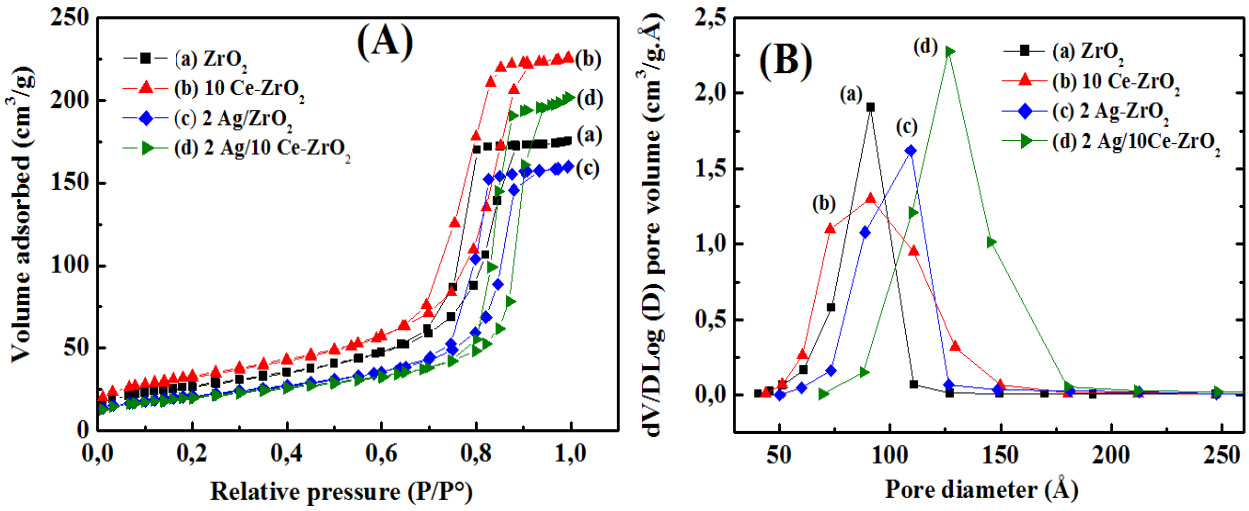

Fig. 1 (A) N_2 adsorption–desorption isotherms and (B) BJH pore size distribution curves of samples

3.2. X-ray diffraction (XRD)

To determine the structural properties of the samples, XRD characterization is performed (Fig. 2). ZrO_2 and Ag/ZrO_2 samples show both the characteristic peaks of the monoclinic and tetragonal phases of ZrO_2 (m-ZrO_2 and t-ZrO_2) at 2θ = 24,38° (110), 28,26° (-111), 31,56° (111), 41,07° (102), 45,21° (-202), 54,09° (300), 55,60 (130), 65,68° (320) [PDF 89-9066] and 2θ = 30,33° (101), 34,67° (002), 50,37° (112), 60,09° (211), 62,57° (202) [PDF 79-1769], respectively. In addition, only the characteristic peaks of the t-ZrO_2 phase are observed on the XRD patterns of Ce-ZrO_2 and Ag/Ce-ZrO_2 samples, is in accordance with our previous work [26], indicating the existence of good synergy between Ce and ZrO_2 which stabilize zirconia at its tetragonal phase. While the diffraction peaks corresponding to CeO_2 crystalline phase are not detected in Ce-ZrO_2 or Ag/Ce-ZrO_2. It means that the support Ce-ZrO_2 has oxygen vacancy on the surface, which leads to the more favourable dispersion of Ag species on Ag/Ce-ZrO_2. This finding correlates with a previous study [36]. On the other hand, XRD patterns of Ag/ZrO_2 catalyst show a peak of very low intensity is located at 2θ = 38, 1° (111) can be assigned the metallic silver (PDF 65-2871). This indicates that silver species are well dispersed on the surface of Ag/ZrO_2 and Ag/Ce-ZrO_2.

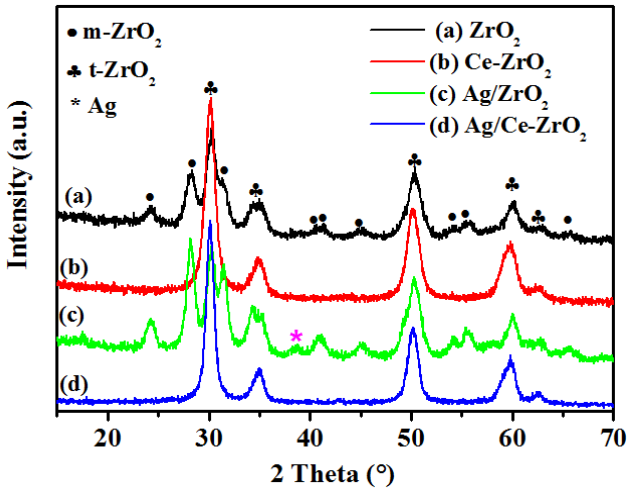

Fig. 2 XRD patterns of samples

3.3. X-ray photoelectron spectroscopy (XPS)

The X-ray photoelectron spectroscopy analysis of Zr, O, Ce and Ag is presented in Fig. 3. Two peaks are observed in the XPS spectra of Zr (3d Fig. 3a) for all the samples at around 181.7 and 184.5 eV and are attributed to $3d_{5/2}$ and $3d_{3/2}$ binding energy of the typical Zr^{4+} state in zirconia [36-38]. Noting that these binding energies appear at different value compared to that of bare ZrO_2 (182.6 eV ($Zr3d_{5/2}$) and 183.6 eV ($Zr3d_{3/2}$) [36] indicating the existence of strong interactions between ZrO_2, cerium and silver species. Similar effect has already been observed for TiO_2 support, modified by V, Ce and SO_4^{2-} species [39].

Fig.3b shows the XPS spectra of O1s of the solids. The Gaussian peaks obtained by deconvolution, at 529.0-529. 9 eV (Fig.3c), correspond to the lattice oxygen (O_L), O^{2-} in the oxygen vacancies (O_V), whereas the O1s binding energies at 530-531.9 eV are related to surface-chemisorbed oxygen species O^- or OH^- [40,41]. It was reported that surface-chemisorbed oxygen is more reactive than lattice one in the oxidation reaction because of its higher mobility [40,41].

The Ce 3d XPS spectrum (Fig. 3d) demonstrates eight peaks (Fig. 3e). The peaks at 885.5 and 904.5 eV correspond to $3d^{10}4f^1$ state of cerium (III) [41,42]. Those located at 900.9, 906.4, 916.9, 917.8, 882.6, and 898.3 eV are related to the $3d^{10}4f^0$ state of cerium (IV) [36,39,41]. So, Ce^{3+} and Ce^{4+} are present on the surface of Ce-ZrO_2 and Ag/Ce-ZrO_2 solids. According to the literature [41], Ce^{4+} 3d and Ce^{3+} 3d are related to lattice oxygen species (O^{2-}) and surface oxygen vacancies, respectively.

The XPS spectra of Ag3d (Fig. 3f) show two peaks of $Ag3d_{5/2}$ and $Ag3d_{3/2}$ binding energy. In fact, the peaks centered at 368.1 and 374.2 eV in the case of Ag/ZrO_2 solid are characteristic of Ag^0 [36,43] and can reveal the predominance of the metallic silver on the surface of this solid. However, the peaks detected at 367.6 and 374 eV for Ag/Ce-ZrO_2 can be attributed to the Ag_2O species [36,43]. From these results, we can underline that the presence of cerium affects the nature and the chemical environment of Ag supported species.

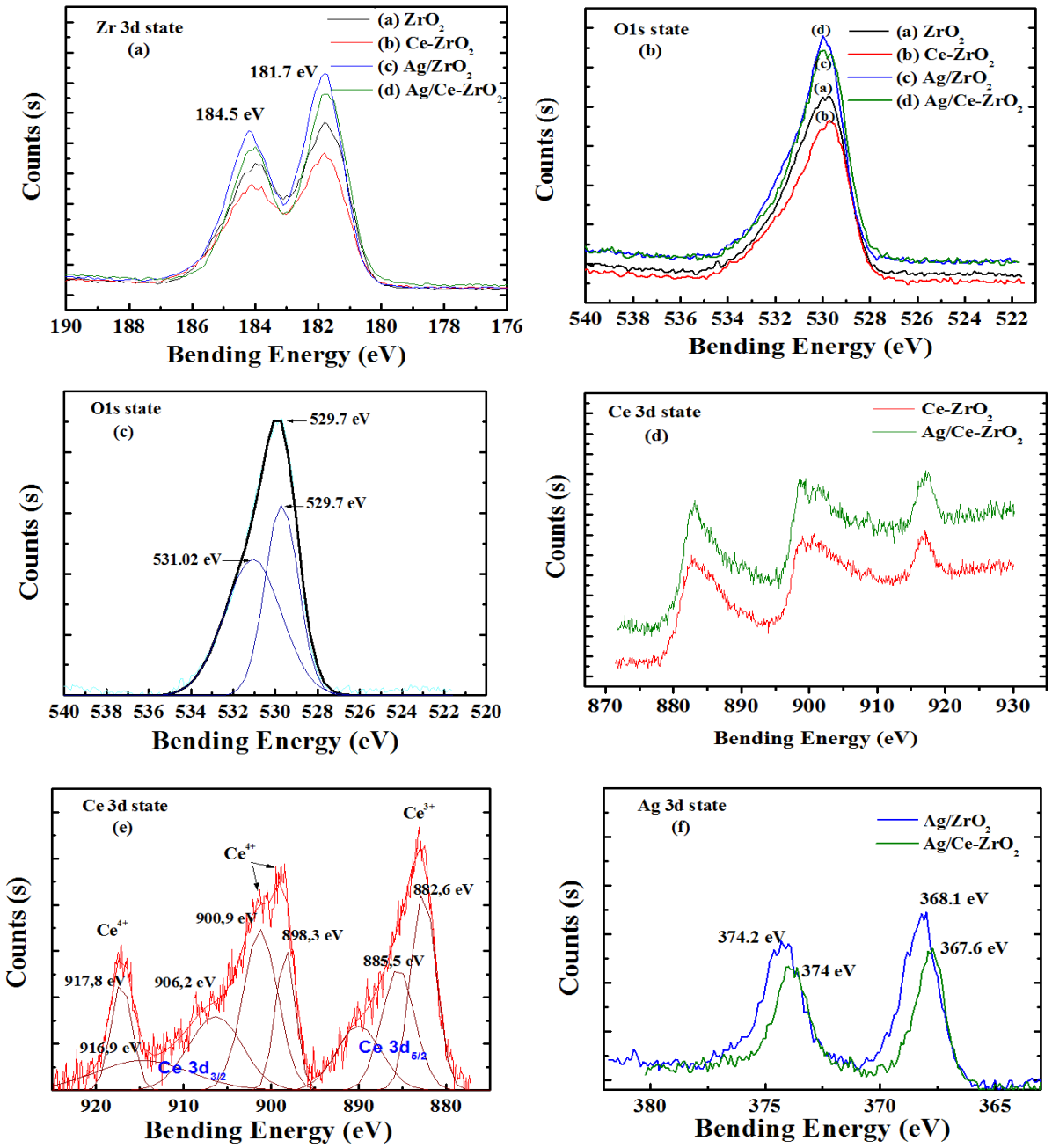

Fig. 3 XPS analysis of samples

3.4. DR UV-vis spectroscopy

The UV-vis spectra of solids are presented in Fig 4. There are several absorption bands in the UV region between 200 and 400 nm for the supports (ZrO_2 and Ce-ZrO_2); however, for the catalysts (Ag/ZrO_2 and Ag/Ce-ZrO_2) the absorption bands are detected in the region between 200 nm and 600 nm. The absorption band situated in 200-250 nm range is attributed to $O^- \rightarrow Zr^{4+}$charge transfer transition [36] and the bands detected in the 230-260 nm and 280-350 nm ranges, on the UV-vis spectra of Ce-ZrO_2 solid are related to $O^{2-} \rightarrow Ce^{3+}$ [36,39,44] and $O^{2-} \rightarrow Ce^{4+}$ [36,39,44]. Two new bands are observed at around 212 and 226 nm in the UV spectrum of Ag/ZrO_2 catalyst and can be attributed to the d-d transitions ($4d^{10}$- $4d^9 5s^1$) of well dispersed Ag^+ ions [36, 44-46]. The bands situated at 290-380 nm for Ag/ZrO_2 and Ag/Ce-ZrO_2 catalysts can be related to the absorptions of $Ag_n^{\delta+}$ clusters [44,45]. Also, there is an important observation referring to the strong absorption band at around ~ 480

nm, corresponding to metallic Ag cluster and aggregates [45]. Based on this UV-vis analysis, we can confirm the existence of highly dispersed Ce and Ag species with a low amount of metallic silver at ZrO_2 surface, which is in agreement with the XRD results. Furthermore, it can be suggested, in agreement with the XPS results and previous reports [36, 45], that the type of support influences the nature and the dispersion of Ag supported species. It seems that the addition of cerium stabilizes the $Ag_n^{\delta+}$ clusters. In fact, a higher intensity of the bands between 290 and 380 (related to $Ag_n^{\delta+}$ form) is obtained in the case of Ag/Ce-ZrO_2 catalyst compared to that of Ag/ZrO_2 sample.

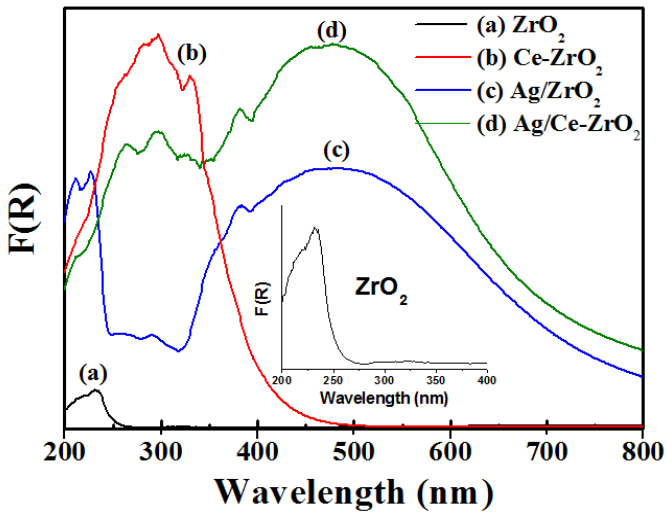

Fig. 4 DRUV-Vis spectra of samples

3.5. Temperature-programmed reduction (H_2-TPR)

To analyse the redox properties of the samples, H_2-TPR analysis was done (Fig. 5). No H_2 consumption peaks are detected for ZrO_2 support because Zr^{4+} is a non-reducible cation [47]. After the addition of cerium, new peaks appeared at low temperature (between 300-500 °C) and are attributed to the reduction of surface cerium species [40,41,44]. When Ag was incorporated into Ce-ZrO_2 and ZrO_2, a new reduction signal appeared at low-temperature (< 200 °C), which is assigned to the reduction of both silver and cerium species. In fact, Zhang J et al. [48] reported that H_2-TPR profile of Ag–CeO_2-A showed two reduction signals at T < 200°C. They have attributed the signal at around ~ 79 °C to O^- or oxygen species reduced to silver, and the reduction peak at around ~103 °C to the reduction of surface O_2 of CeO_2 interacting with silver. Noting that after the addition of Ag to Ce-ZrO_2 solid, the reduction peaks of Ce species happen at lower temperature. This result suggests that silver promotes the reduction of surface oxygen of CeO_2, as explained previously by Qu Z et al. [44]. These H_2-TPR results indicate that the addition of Ce and/or Ag leads to the creation of many redox sites at ZrO_2 surface [41,49].

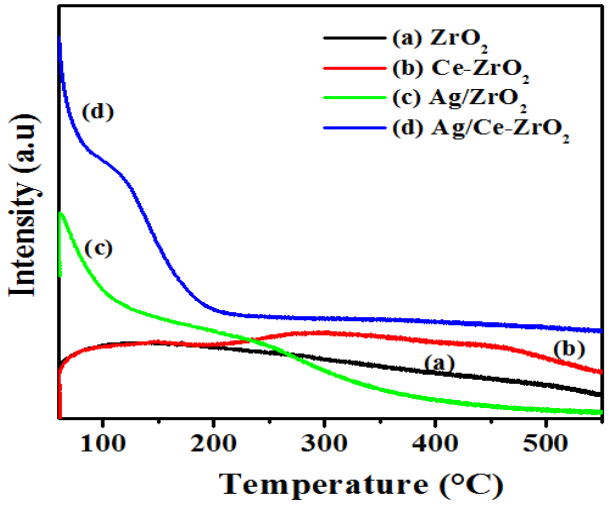

Fig. 5 H_2-TPR analysis of samples

3.6. Temperature programmed desorption of O_2 (O_2-TPD)

The O_2-TPD experiments were performed to study the interactions between Ce, Ag and oxygen and the results are shown in Fig. 6. The Ag/ZrO_2 exhibit a wide O_2 desorption peak at around ~ 235 °C could be attributed to the weak adsorption molecular oxygen adsorbed on a silver surface [50,51]. Nevertheless, the O_2-TPD profile of $Ag/Ce\text{-}ZrO_2$ shows three oxygen desorption peaks at around 150, 330 and 440 °C. According to ref [50-52], the desorption peak at 150 °C should be attributed to the weak adsorption molecular oxygen; the desorption peak appeared at 330 °C should be ascribed to the chemically adsorbed oxygen on the surface and the desorption peak appearing at 440 °C should be assigned to the chemically adsorbed oxygen in the oxygen vacancy. Thus, this result implies that there is a large content of the adsorbed oxygen species on the $Ag/Ce\text{-}ZrO_2$ catalyst, certainly due to the presence of cerium known by its high oxygen storage capacity. Furthermore, it is reasonable to suggest that the interaction between Ag and $Ce\text{-}ZrO_2$ can influence the number of surface oxygen and therefore the number of active sites, which is well consistent with the H_2-TPR analysis. From this result, we can conclude that the $Ag/Ce\text{-}ZrO_2$ surface can promote the adsorption and activation of gaseous oxygen.

It is well known that the lattice oxygen plays a crucial role in the catalytic oxidation reaction of VOCs, and the increase of surface lattice oxygen can improve the catalytic oxidation. Previous reports [41,44], showed that the presence of larger amounts of surface adsorbed oxygen (O_2^- or O^-), plays an important role in the stability and dispersion of silver species, and, consequently, enhances the complete oxidation of VOCs.

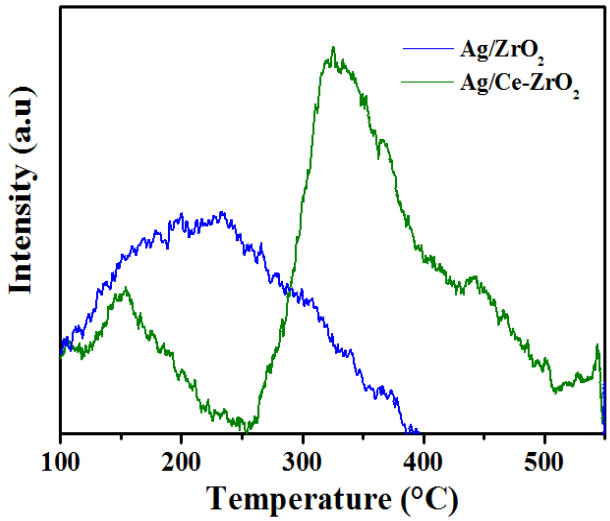

Fig. 6 O_2-TPD analysis of samples

3.7. Temperature-programmed desorption (NH_3-TPD)

Temperature-programmed desorption of ammonia (NH_3-TPD) is a useful method for studying the acidity of solids. Fig.7 displays the NH_3-TPD profiles of materials. The NH_3-TPD profiles of ZrO_2 and Ce-ZrO_2 exhibit a broad NH_3 desorption peak between 100 and 400 °C, which can assign to the desorption of ammonia from weak and medium strong acid sites [53,54]. It can be noticed that the intensity of this peak is higher for the solid containing cerium compared to that of the bare zirconia connected with the incorporation of Ce, which increases the total acidity of the support. This is consistent with our previous work [26]. Furthermore, the addition of silver induces a progressive transformation of the surface acidity of ZrO_2 and Ce-ZrO_2 supports, it leads to a decrease of the intensity of NH_3 desorption peak situated in the 100-400 °C temperature range, but creates a new strong acid sites at higher temperature (desorption of NH_3 at T > 400 °C), particularly for Ag/Ce-ZrO_2 catalyst. The transformation of the surface acidity of support after deposition of the active phases has been observed for other type of catalysts and can be explained by the existence of a strong interaction between the support and the supported species [26,46].

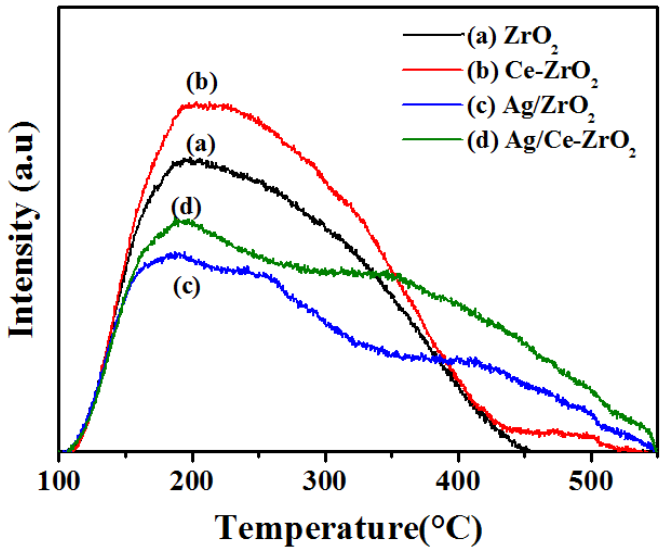

Fig. 7 NH_3-TPD analysis of samples

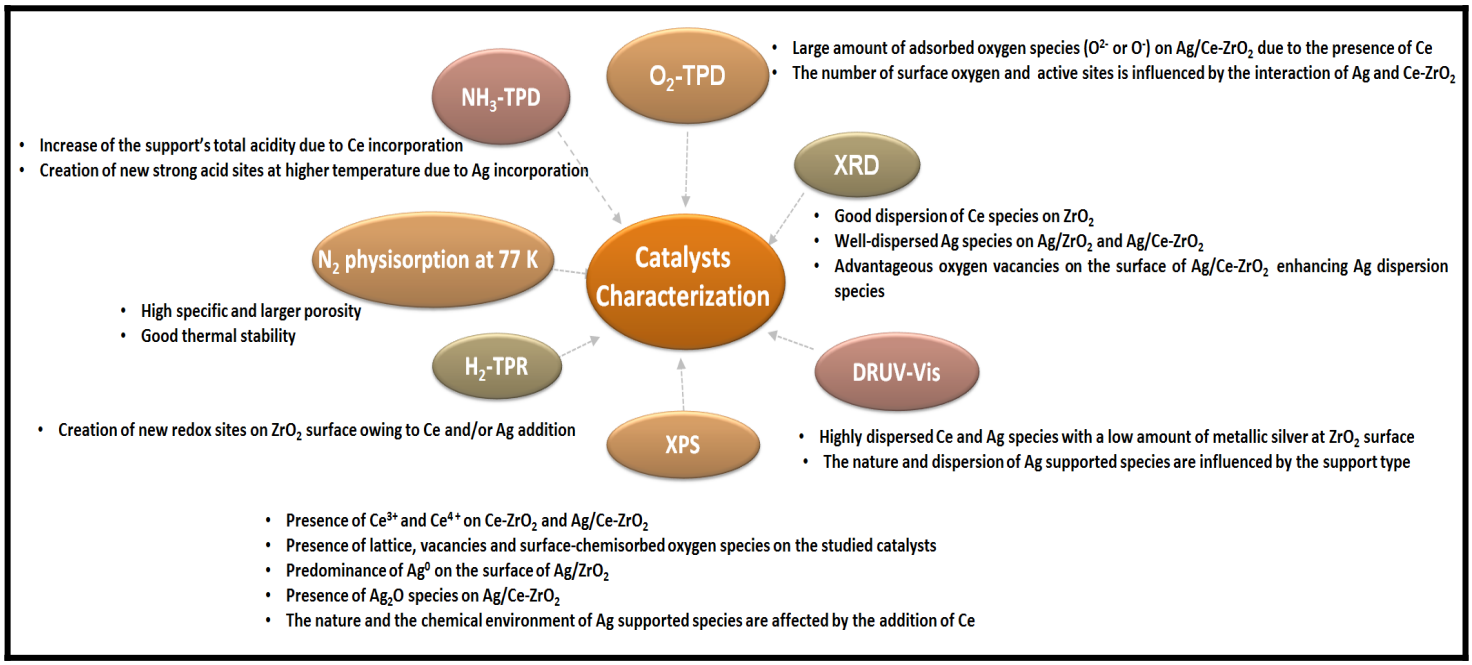

Scheme 1. Summary of characterization results provided by the different employed techniques.

4. Evaluation of Catalyst activity

Fig. 8A and 8B show the performance of the as-prepared samples (ZrO_2, $AgZrO_2$, Ce-ZrO_2 and Ag-Ce-ZrO_2) for the low temperature catalytic oxidation of the toluene (toluene concentration =1000 ppm, weight hourly space velocity (WHSV) = 60,000 h^{-1}). The values of the temperatures of toluene conversion of 10 %, 50 % and 90 % were named T10 %, T50 % and T90 % (see table 2). As shown in Fig. 8A, the ZrO_2 support possesses low activity in the total oxidation of C_7H_8. The addition of cerium enhances the low-temperature toluene oxidation activity, with improvement of T10 % and T50 % to 344 °C and 437 °C respectively, (see table 2). It is Obviously observed that, after the addition of Ag, the catalytic performance of the Ag/ZrO_2 and Ag/Ce-ZrO_2 catalysts was greatly improved, and the T90% shifted to 376 °C and 331 °C, respectively (see table 2). Ag/Ce-ZrO_2 possessed better catalytic activity at low temperature compared to Ag/ZrO_2. 100% C_7H_8 conversion to CO_2 is achieved between 300 and 550 °C over Ag/Ce-ZrO_2 sample. Such behavior is explained by the crucial role of cerium species (excellent oxygen storage capacity) which are in good interaction with Ag species. It is well known that oxygen species in transition metal oxides are the key factor in VOC oxidation. Researchers reported that the doping of transition metal oxide catalysts with noble or transition metal can change the physicochemical properties of the material (morphology, surface area and oxygen species), and the interaction enhances the catalytic activity [26,55-59]. Therefore, we can demonstrate that the incorporation of Ag species increases the content of surface lattice oxygen species and its migration (from the bulk to the surface) and consequently facilitates the low-temperature activity of toluene oxidation over Ag/Ce-ZrO_2. Combined with the results of H_2-TPR, O_2-TPD and NH_3-TPD characterization, it reveals that Ag/Ce-ZrO_2 possessed more oxygen vacancy (from O_2-TPD results) which promotes the dispersion of Ag on the support surface. The good dispersion of silver on Ce-ZrO_2 leads to the strong interaction between Ag and Ce, which induces better reduction ability at low temperature (from H_2-TPR) and creates new strong acid sites (from NH_3-TPD). Thus, we can conclude that lower reduction temperature and abundant surface-active oxygen (crucial role of Ce in VOC oxidation),

originating from the strong synergy effect between Ce and Ag, are responsible for the excellent catalytic performance of Ag/Ce-ZrO_2.

It is found that the oxidation of volatile organic compounds (VOCs) over solid oxide catalysts follows the Mars-van Krevelen [60-65], in which the lattice oxygen species reacts with reactant molecules and at the same time are replenished by the oxygen vacancies containing gaseous phase [66]. It means that the surface adsorbed oxygen and lattice oxygen played an important role in the oxidation process, which promoted the adsorption, activation and oxidation of toluene, and especially the breakage of aromatic rings.

In summary, based on the above knowledge, results and discussion, Ag/Ce-ZrO_2 enhances the amount of activated oxygen (presence of Ce), which may contribute to the acceleration of the adsorption of toluene. What is more, Ag species facilitates the transfer of lattice oxygen, provides more active lattice oxygen, and consequently improves the cycle of oxygen species. So, in this case, the mechanism of the reaction could be explained as follows: First, the toluene molecule was adsorbed on active site (Ag species) to form the interface between Ag and toluene. The Ag-C_7H_8 reacts with lattice oxygen on the surface to form CO_2 and H_2O. Then the gaseous oxygen reoxidates the catalyst.

Table 2: Conversion of toluene at different temperatures over the catalysts

Catalyst	ZrO_2	Ce-ZrO_2	Ag/ZrO_2	Ag/Ce-ZrO_2
T10 %	470 °C	344 °C	344 °C	312 °C
T50 %	550 °C	437 °C	360 °C	320 °C
T90 %	-	513 °C	376 °C	331 °C

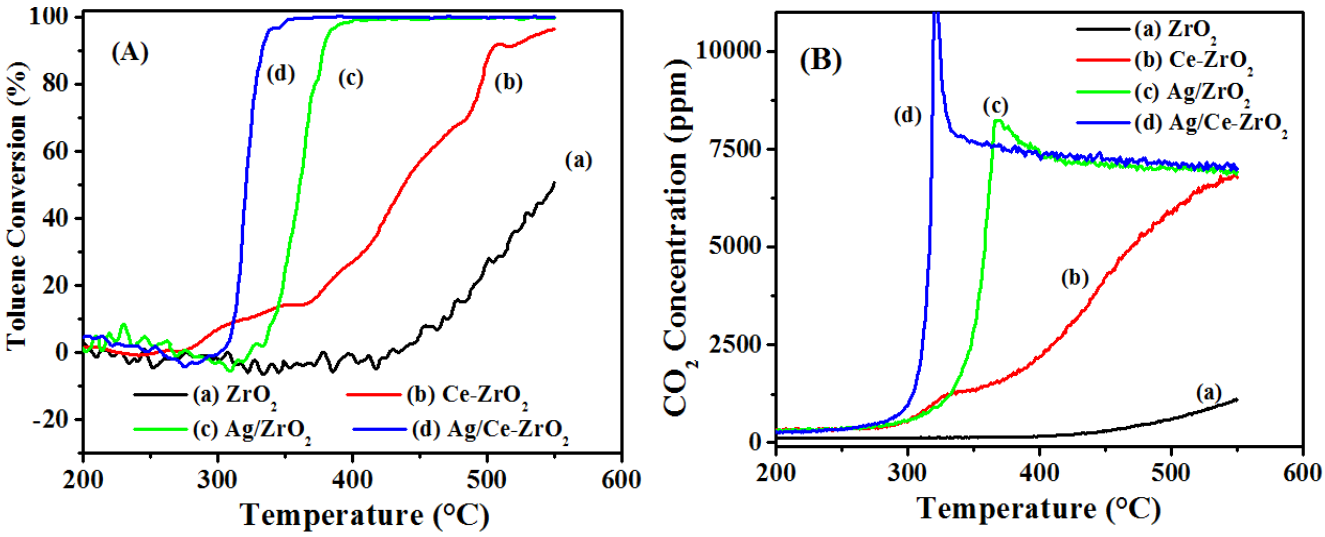

Fig. 8 (A) Toluene conversion and (B) CO_2 formation (ppm) over the samples

5. Conclusion

In this work, a new Ag/Ce-ZrO_2 catalyst for total oxidation of toluene in the presence of water vapor was performed. A complete C_6H_5-CH_3 conversion to CO_2 is obtained in a wide temperature range (300-550 °C) over Ag/Ce-ZrO_2 catalyst. Ag/Ce-ZrO_2 shows improved low-temperature oxidation than the Ag/ZrO_2. Especially, the conversion of the toluene on the Ag/Ce-ZrO_2 shifted to lower temperature (T90 % = 331 °C) than Ag/ZrO_2 (T90% = 376 °C). Characterization results showed that good reduction ability at low temperature, strong interaction between Ag species Ce species and more oxygen species are responsible for the best catalytic activity of Ag/Ce-ZrO_2 catalyst.

Declarations

Acknowledgements

This study was supported by the ministry of higher education and scientific research of Tunisia.

Conflict of interest

The authors declare that there is no conflict of interest regarding the publication of this article.

Ethical Approval

Not applicable

Funding

Not applicable

References

[1] L. Bao, S. Zhu, Y. Chen, Y. Yang, W. Meng, S. Xu, Z, Lin, X. Lin, M.Sun, L. Guo , Anionic defects engineering of Co_3O_4 catalyst for toluene oxidation, Fuel 314 (2022) 122774

[2] L.F. Liotta, Catalytic oxidation of volatile organic compounds on supported noble metals, Appl. Catal. B: Environ. 100 (2010) 403–412.

[3] M.A. Bari, W.B. Kindzierski, Ambient volatile organic compounds (VOCs) in Calgary, Alberta: sources and screening health risk assessment, Sci. Total Environ. 631-632 (2018) 627–640.

[4] J.V. Durme, J. Dewulf, W. Sysmans, C. Leys, H.V. Langenhove, Abatement and degradation pathways of toluene in indoor air by positive corona discharge, Chemosphere 68 (2007) 1821–1829

[5] X.Y. Shi, X.D. Zhang, F.K. Bi, Z.H. Zheng, L.J. Sheng, J.C. Xu, Z. Wang, Y.Q. Yang, Effective toluene adsorption over defective UiO-66-NH_2: an experimental and computational exploration, J. Mol. Liq. 316 (2020), 113812.

[6] T. Chang, J.Q. Lu, Z.X. Shen, Y. Huang, D. Lu, X. Wang, J.J. Cao, R. Morent, Simulation and optimization of the post plasma-catalytic system for toluene degradation by a hybrid ANN and NSGA-II method, Appl. Catal. B: Environ. 244 (2019) 107–119.

[7] X.X. Xu, P.T. Wang, W.C. Xu, J.L. Wu, L.M. Chen, M.L. Fu, D.Q. Ye, Plasma-catalysis of metal loaded SBA-15 for toluene removal: Comparison of continuously introduced and adsorption-discharge plasma system, Chem. Eng. J. 283 (2016) 276-284.

[8] C.A.B. K.B. Schnelle Jr., Air Pollution Control Technology Handbook, Crc Press, 2001

[9] N. Jiang, N. Lu, K.F. Shang, J. Li, Y. Wu, Innovative approach for benzene degradation using hybrid surface/packed-bed discharge plasmas, Environ. Sci. Technol. 47 (2013) 9898-9903

[10] X.B. Zhu, S. Zhang, Y. Yang, C.H. Zheng, J.S. Zhou, X. Gao, X. Tu, Enhanced performance for plasma-catalytic oxidation of ethyl acetate over La1-xCexCoO$_{3}^{+\delta}$ catalysts, Appl. Catal. B: Environ. 213 (2017) 97-105.

[11] A. Maciuca, C. Batiot-Dupeyrat, J.-M. Tatibouët, Synergetic effect by coupling photocatalysis with plasma for low VOCs concentration removal from air, Appl. Catal. B: Environ. 125 (2012) 432-438.

[12] R. Balzer, L F D. Probst, V. Drago, W.H. Schreiner and H. V. Fajardo. Catalytic oxidation of volatile organic compaounds (n-hexane, Benzene, Toluene, o-Xylene) promoted by cobalt catalysts supported on γ-Al_2O_3-CeO_2. Braz J Chem Eng. 31 (2014) 757-769

[13] K. Zeng, Y.T. Wang, C.F. Huang, H.C. Liu, X.H. Liu, Z. Wang, J. Yu, C.H. Zhang, Catalytic combustion of propane over MnNbOx composite oxides: the promotional role of niobium, Ind. Eng. Chem. Res. 60 (2021) 6111–6120.

[14] C.H. Zhang, H.J. Cao, C. Wang, M.X. He, W.C. Zhan, Y.L. Guo, Catalytic mechanism and pathways of 1, 2-dichloropropane oxidation over $LaMnO_3$ perovskite: an experimental and DFT study, J. Hazard. Mater. 402 (2021), 123473.

[15] K.Y. Zhang, L.Y. Dai, Y.X. Liu, J.G. Deng, L. Jing, K.F. Zhang, Z.Q. Hou, X. Zhang, J. Wang, Y. Feng, Y.X. Zhang, H.X. Dai, Insights into the active sites of chlorineresistant Pt-based bimetalliccatalysts for benzene oxidation, Appl. Catal. B: Environ. 279 (2020), 119372.

[16] C.H. Zhang, Y.T. Wang, G.Q. Li, L. Chen, Q.S. Zhang, D. Wang, X.B. Li, Z. Wang, Tuning smaller Co_3O_4 nanoparticles onto HZSM-5 zeolite via complexing agents for boosting toluene oxidation performance, Appl. Surf. Sci. 532 (2020), 147320.

[17] X.D. Zhang, X.T. Lv, F.K. Bi, G. Lu, Y.X. Wang, Highly efficient Mn_2O_3 catalysts derived from Mn-MOFs for toluene oxidation: the influence of MOFs precursors, Mol. Catal. 482 (2020), 110701.

[18] X.D. Zhang, Y. Yang, Q. Zhu, M.D. Ma, Z.Y. Jiang, X. Liao, C. He, Unraveling the effects of potassium incorporation routes and positions on toluene oxidation over α-MnO_2 nanorods: based on experimental and density functional theory (DFT) studies, J. Colloid Interf. Sci. 598 (2021) 324–338.

[19] Y. Lin, J. Sun, S.J. Li, D. Wang, C.H. Zhang, Z. Wang, X.B. Li, An efficient Pt/ CeyCoOx composite metal oxide for catalytic oxidation of toluene, Catal. Lett. 150 (2020) 3206–3213.

[20] S.J. Li, Y. Lin, D. Wang, C.H. Zhang, Z. Wang, X.B. Li, Polyhedral cobalt oxide supported Pt nanoparticles with enhanced performance for toluene catalytic oxidation, Chemosphere 263 (2021), 127870.

[21] Z. Wang, S.J. Li, C.H. Zhang, D. Wang, X.B. Li, The opportunities and challenges for NH3 oxidation with 100% conversion and selectivity, Catal. Surv. Asia 25 (2021) 103–113.

[22] Sung Hyok Ri , Fukun Bi , Aili Guan , Xiaodong Zhang , Manganese-cerium composite oxide pyrolyzed from metal organic framework supporting palladium nanoparticles for efficient toluene oxidation, Journal of Colloid and Interface Science 586 (2021) 836–846.

[23] Y.F. Li, L.J. Xiao, F.F. Liu, Y.S. Dou, S.M. Liu, Y. Fan, G. Cheng, W. Song, J.L. Zhou, Core-shell structure Ag@ Pd nanoparticles supported on layered MnO_2 substrate as toluene oxidation catalyst, J. Nanopart. Res. 21 (2019) 28.

[24] D.B. Wang, F.Y. Jia, H. Wang, F. Chen, Y. Fang, W.B. Dong, G.M. Zeng, X.M. Li, Q. Yang, X.Z. Yuan, Simultaneously efficient adsorption and photocatalytic degradation of tetracycline by Fe-based MOFs. J. Colloid Interf. Sci. 519 (2018) 273- 284

[25] W.B. Dong, D.B. Wang, H. Wang, M.K. Li, F. Chen, F.Y. Jia, Q. Yang, X.M. Li, X.Z. Gong, H.L. Li, J. Ye, Facile synthesis of In2S3/UiO-66 composite with enhanced adsorption performance and photocatalytic activity for the removal of tetracycline under visible light irradiation. J. Colloid Interf. Sci. 535 (2019) 444-457

[26] R. Ismail, J. Arfaoui, Z. Ksibi, A. Ghorbel, G. Delahay. Ag/ZrO_2 and $Ag/Fe–ZrO_2$ catalysts for the low temperature total oxidation of toluene in the presence of water vapor, Transit Met Chem. 45 (2020) 501–509

[27] R. Ismail, J. Arfaoui, Z. Ksibi, A. Ghorbel, G. Delahay, Effect of the iron amount on the physicochemical properties of $Fe–ZrO_2$ aerogel catalysts for the total oxidation of Toluene in the presence of water vapor, Journal of Porous Materials 27 (2020) 1847–1852

[28] J.A. Zhu, W.R. Zhang, Q.P. Qi, H.W. Zhang, Y.Q. Zhang, D.K. Sun, P. Liang, Catalytic oxidation of toluene, ethyl acetate and chlorobenzene over Ag/MnO_2- cordierite molded catalyst. Sci. Rep. 9 (2019) 12162.

[29] J. Chen, X. Chen, X. Chen, W.J. Xu, Z. Xu, H.P. Jia, J. Chen, Homogeneous introduction of CeOy into MnOx-based catalyst for oxidation of aromatic VOCs, Appl. Catal. B: Environ. 224 (2018) 825–835.

[30] Y.W. Jiang, J.H. Gao, Q. Zhang, Z.Y. Liu, M.L. Fu, J.L. Wu, Y. Hu, Enhanced oxygen vacancies to improve ethyl acetate oxidation over $MnOx-CeO_2$ catalyst derived from MOF template, Chem. Eng. J. 371 (2019) 78–87.

[31] X.J. Zhang, J.G. Zhao, Z.X. Song, W. Liu, H. Zhao, M. Zhao, Y. Xing, Z.A. Ma, H. X. Du, The catalytic oxidation performance of toluene over the Ce-Mn-Ox catalysts: effect of synthetic routes, J. Colloid Interf. Sci. 562 (2020) 170–181.

[32] Y.J. Luo, D.F. Lin, Y.B. Zheng, X.S. Feng, Q.H. Chen, K. Zhang, X.Y. Wang, L. L. Jiang, MnO2 nanoparticles encapsuled in spheres of Ce-Mn solid solution: efficient catalyst and good water tolerance for low-temperature toluene oxidation, Appl. Surf. Sci. 504 (2020), 144481.

[33] KSW Sing. Reporting physisorption data for gas/solid systems with special reference to the determination of surface area and porosity, Pure and Appl Chem 57 (1985) 603-619

[34] M. Kruk, M. Jaroniec. Gas Adsorption Characterization of Ordered Organic-Inorganic Nanocomposite Materials. Chem Mater. 13 (2001) 3169-3183.

[35] W. Khaodee, N. Tangchupong, B. Jongsomjit, P. Praserthdam and S. Assabumrungrat, A study on isosynthesis via CO hydrogenation over $ZrO_2–CeO_2$ mixed oxide catalysts. Catal Commun 10 (2009) 494-501.

[36] Z. Guerra-Que, G. Torres-Torres, H. Pérez-Vidal, I. Cuauhtémoc-Lopez, A. Espinosa de los Monteros, J.N. Beltramini, D.M. Frias-M´arquez. Silver nanoparticles supported on zirconia–ceria for the catalytic wet air oxidation of methyl tert-butyl ether. RSC Adv. 7 (2017) 3599-3610.

[37] S. Ardizzone, M.G. Cattania, P. Lugo. Interfacial electrostatic behaviour of oxides: Correlations with structural and surface paramaters of the phase. Electrochim Acta.39 (1994) 1509-1517.

[38] S. Ardizzone, C.L .Bianchi, M. Signoretto. Zr_(IV) surface chemical state and acid features of sulphated-zirconia samples. Appl Surf Sci, 136 (1998) 136: 213-220.

[39] J. Arfaoui, A. Ghorbel, C. Petitto, G. Delahay. Novel $V_2O_5-CeO_2-TiO_2-SO_4^{2-}$ nanostructured aerogel catalyst for the low temperature selective catalytic reduction of NO by NH_3 in excess O_2, Appl Catal B Environ.224 (2018) 264-275.

[40] M. Piumetti, S. Bensaid, N. Russo, D. Fino. Nanostructured ceria-based catalysts for soot combustion: investigations on the surface sensitivity. Appl Catal B Environ. 165 (2015) 742-751.

[41] S. Wu, Y. Yang, C. Lu, Y. Ma, S. Yuan, G. Qian. Soot oxidation over CeO_2 or Ag/CeO_2: influences of bulk oxygen vacancies and surface oxygen vacancies on activity and stability of catalyst. (2018). https://doi.org/10.1002/ejic.201800423

[42] X. Wu, L. Xu, D. Weng. The thermal stability and catalytic performance of Ce-Zr promoted Rh-Pd/g-Al_2O_3 automotive catalysts. Appl Surf Sci. 221 (2004) 375-383.

[43] Li H, Duan X, Liu G, Liu X. Photochemical synthesis and characterization of Ag/TiO_2 nanotube composites. J Mater Sci, 2008, 43:1669-1676.

[44] Z. Qu, F. Yu, X. Zhang,Y. Wang, J. Gao. Support effects on the structure and catalytic activity of mesoporous Ag/CeO_2 catalysts for CO oxidation. Chem Eng J. 229 (2013) 522-532.

[45] K A Bethke, H H Kung. Supported Ag Catalysts for the Lean Reduction of NO with C_3H_6. J Catal. 172 (1997) 93-102.

[46] L. Kundakovic, M. Flytzani-Stephanopoulos. Deep oxidation of methane over zirconia supported Ag catalysts. Appl Catal A Gen. 183 (1999) 35-51.

[47] Z. Yan′e, W. Xing, Zua, L. Kongzhai, W. Yuhao , W. Yonggang . Characteristic of macroporous CeO_2-ZrO_2 oxygen carrier for chemical-looping steam methane reforming. J Rare Earth. 32 (2014) 842-848.

[48] J. Zhang, L. Li, X. Huang, G. Li. Fabrication of Ag–CeO_2 core–shell nanospheres with enhanced catalytic performance due to strengthening of the interfacial interactions. J Mater Chem. 22 (2012) 10480-10487.

[49] A M. Hengne, A V Malawadkar, N S Biradar, C V Rode. Surface synergism of Ag-Ni-ZrO_2 nanocomposite for catalytic transfer hydrogenation of bio-derived platform molecules. RSC Adv. 4 (2012) 9730-9736.

[50] S. Zh. Todorova, H G Kolev, M .G.Shopska, G.B. Kadinov, J.P. Holgado, A. Caballero. Silver-based catalysts for preferential CO oxidation in hydrogen-rich gases (PROX). Bulg Chem Commun. 2018; 50: 17-23.

[51] Y E. Sung, W.Y. Lee, H.K. Rhee, H I.Lee. the effect of oxygen on the chemisorption on polycrystalline silver surface. Kor J Chem Eng. 6 (1989) 300-305

[52] L. Kongzhai, W. Hua, W. Yonggang, L. Mingchun. Catalytic performance of cerium iron complex oxides for partial oxidation of methane to synthesis gas, J. Rare EARTH. 26 (2008) 705-710.

[53] C. Petitto, H P Mutin, G Delahay. Hydrothermal activation of silver supported alumina catalysts prepared by sol–gel method: Application to the selective catalytic reduction (SCR) of NOx by n-decane. Appl. Catal. B. 134-135 (2013) 258-264.

[54] J. Arfaoui, L K. Boudali, A. Ghorbel. Catalytic epoxidation of allylic alcohol (E)-2-Hexen-1-ol over vanadium supported on unsulfated and sulfated titanium pillared montmorillonite catalysts: Effect of sulfate groups and vanadium loading. Appl Clay Sci. 48 (2010) 171-178.

[55] B. Solsona, T. Garcia, S. Agouram, G.J. Hutchings, S.H. Taylor, The effect of gold addition on the catalytic performance of copper manganese oxide catalysts for the total oxidation of propane, Appl. Catal. B Environ. 101 (2011) 388–396.

[56] H. Yang, J. Deng, S. Xie, Y. Jiang, H. Dai, C.T. Au, Au/MnOx/3DOM SiO_2: Highly active catalysts for toluene oxidation, Appl. Catal. A Gen. 507 (2015) 139–148.

[57] J. Chen, X. Chen, X. Chen, W. Xu, Z. Xu, H. Jia, J. Chen, Homogeneous introduction of CeOy into MnOx-based catalyst for oxidation of aromatic VOCs, Appl. Catal. B Environ. 224 (2018) 825–835.

[58] K. Yamazaki, T. Kayama, F. Dong, H. Shinjoh, A mechanistic study on soot oxidation over CeO_2–Ag catalyst with 'rice-ball' morphology, J. Catal. 282 (2011) 289–298.

[59] K. Choi, D. Lee, H. Kim, Y. Yoon, C. Park, Y. Kim, Reaction characteristics of precious-metal-free ternary MnCuM (M = Ce Co, Cr, and Fe) oxide catalysts for low-temperature CO oxidation, Ind. Eng. Chem. Res. 55 (2016) 4443–4450.

[60] Y. Qin, H. Wang, C. Dong, Z. P. Qu, Evolution and enhancement of the oxygen cycle in the catalytic performance of total toluene oxidation over manganese-based catalysts, J. Catal. 380 (2019) 21-31.

[61] C. G. Zhang, W. Chu, F. Chen, L. Li, R. Y. Jiang, J. L. Yan, Effects of cerium precursors on surface properties of mesoporous CeMnOx catalysts for toluene combustion, J. Rare earths 38 (2020) 70-75.

[62] Y. Qin, Z. Qu, C. Dong, N. Huang. Effect of pretreatment conditions on catalytic activity of Ag/SBA-15 catalyst for toluene oxidation. Chinese J Catal, 38 (2017) 1603-1612.

[63] J. Li, Z. Qu, Y. Qin, H. Wang. Effect of MnO_2 morphology on the catalytic oxidation of toluene over Ag/MnO_2 catalysts. Appl Surf Sci. 385 (2016) 234-240.

[64] B. Dou , D. Yang , T. Kang , Y. Xu , Q. Hao , F. Bin , X. Xu, Morphology effects of CeO_2-ZrO_2 on the catalytic performance of CuO/ CeO_2-ZrO_2 for toluene oxidation, Carbon Resources Conversion 4 (2021) 55–60.

[65] S. Hyok Ri, F. Bi, A. guan, X. Zhang, Manganese-cerium composite oxide pyrolyzed from metal organic framework supporting palladium nanoparticles for efficient toluene oxidation, Journal of Colloid and Interface Science (2020), doi: https://doi.org/10.1016/j.jcis.2020.11.008.

[66] Z. Ren, Z. Wu, W. Song, W. Xiao, Y. Guo, J. Ding, S.L. Suib, P.-X. Gao, Low temperature propane oxidation over Co_3O_4 based nano-array catalysts: Ni dopant effect, reaction mechanism and structural stability, Appl. Catal. B Environ. 180 (2016) 150–160.